Non-linear evolution and acceleration of unstable fuel-lean hydrogen/air flame at ambient and cryogenic temperatures

Linlin Yang[a,c], Tianhan Zhang[b], Yiqing Wang[a], Xiaohang Fang[c,d], Felix Leach[c], Zheng Chen[a,*]

[a] *College of Engineering, Peking University, Beijing, 100871, China*
[b] *AI for Science Institute, Beijing, 100080, China*
[c] *Department of Engineering Science, University of Oxford, Oxford, OX1 3PJ, UK*
[d] *Department of Mechanical & Manufacturing Engineering, Schulich School of Engineering, University of Calgary, Calgary, T2L 1Y6, Canada*

Abstract

Hydrogen storage at cryogenic temperatures is crucial for industrial applications, yet these conditions can significantly affect flame behavior. Both Darrieus-Landau instability (DLI) and diffusional-thermal instability (DTI) can intensify at cryogenic temperature, leading to unique flame dynamics relevant to safe hydrogen usage. In this study, two-dimensional simulations are performed to assess the effects of cryogenic temperature on the non-linear evolution and acceleration of fuel-lean hydrogen/air flames. By changing the initial temperature and equivalence ratio of the unburned gas as well as the channel width, distinct flame evolution regimes driven by the interplay of DLI and DTI are identified. Specifically, for fuel-lean hydrogen/air flames, the growth rate of DLI and DTI in the linear stage increases at cryogenic temperatures. In the non-linear stage, DTI leads to the chaotic evolution of the cellular flame, which is further destabilized at cryogenic temperatures. It is found that the long-term dynamics, characterized by cell splitting, merging, and lateral movement, result from complex interactions among flow, flame stretch, and chemical reactions. Moreover, flame structure analysis shows that, compared to ambient temperatures, cryogenic temperatures significantly increase the local reaction rate. The propagation speed of fuel-lean

*Corresponding Author
Email address: cz@pku.edu.cn (Zheng Chen)

hydrogen/air flames is further accelerated at cryogenic temperature, which is associated with the combined effects of enhanced local reaction rate and increased flame surface area, with the primary contribution from enhanced DTI and the secondary contribution from enhanced DLI. In contrast, stoichiometric and fuel-rich flames propagate in a stable single-cusp shape, with their acceleration primarily driven by DLI and flame surface area increase. The width of the channel also affects cellular flame evolution. Rather than altering reaction rates, channel geometry influences flame acceleration mainly through constraining the surface area during flame propagation. These insights contribute to our understanding of cryogenic hydrogen flame dynamics and have important implications for hydrogen safety management.

Keywords: Hydrogen flame, Cryogenic temperature, Cellular instabilities, Non-linear evolution

---

Novelty and Significance Statement

The novelty of this study lies in assessing and interpreting the effects of cryogenic temperatures on fuel-lean hydrogen/air flames subjected to both Darrieus-Landau instability (DLI) and diffusional-thermal instability (DTI) for the first time. Through detailed numerical simulations, we reveal mechanisms driving the chaotic evolution and cellular structure of flame fronts under cryogenic conditions. Our quantitative analysis demonstrates the relative contributions of DLI and DTI. The research fills a critical knowledge gap by examining the role of DLI and DTI at cryogenic conditions for highly unstable fuel-lean hydrogen/air flame. The results are especially valuable for predicting and managing potential flame acceleration hazards in cryogenic hydrogen systems, where traditional ambient-temperature models may not adequately capture the underlying physics.

Author Contributions Statement

- L. Yang: Conceptualization, Methodology and formal analysis, Writing – original draft, Writing –review & editing
- T. Zhang: Assisted in further analysis, Writing – review & editing.
- Y. Wang: Assisted in further analysis, Writing – review & editing.

- X. Fang: Assisted in further analysis, Funding acquisition, Writing – review & editing.
- F. Leach: Assisted in further analysis, Funding acquisition, Writing – review & editing.
- Z. Chen: Conceptualization, Methodology, Writing –review & editing, Funding acquisition, Supervision.

1. Introduction

Recently, hydrogen has received great attention for its potential to reduce carbon dioxide emissions [1, 2]. Cryogenic storage and hydrogen transportation are necessary for some applications due to gaseous hydrogen's low volumetric energy density. Due to the low minimum ignition energy and high diffusivity and reactivity, safety issues related to cryogenic hydrogen pose a serious problem to hydrogen utilization [3]. After accidental release, liquid hydrogen can evaporate rapidly and mix with ambient air [4], forming a cryogenic premixed hydrogen/air mixture, leading to possible deflagration after ignition [5]. Moreover, the onset of flame instabilities may lead to the deflagration-to-detonation transition (DDT) through flame acceleration, causing faster energy release and more severe damage [6–8]. Therefore, it is important to understand the propagation and acceleration of hydrogen/air flames subject to instabilities at cryogenic temperatures.

In the absence of gravity [9], intrinsic flame front instabilities including Darrieus-Landau instability (DLI, or hydrodynamic instability) and diffusional-thermal instability (DTI) [10–13], can greatly accelerate the flame propagation through flame front wrinkling. Under cryogenic conditions, the DLI can be enhanced as the expansion ratio (density ratio of unburned to burned gas, i.e., $\sigma = \rho_u/\rho_b$) becomes large [14]. The DTI can also become significant since the Zel'dovich number increases with decreasing temperature for fuel-lean hydrogen/air flames with sub-unity Lewis number ($Le < 1$) [11, 15]. Previous studies [7, 16, 17] demonstrated that DLI at cryogenic temperatures can be much stronger than that at ambient temperatures for stoichiometric hydrogen/air flame. For turbulent flames, the effect of DLI on flame acceleration was studied by Chen *et al.* [18]. These studies show that a large expansion ratio at cryogenic temperatures causes strong flame acceleration. In the recent work by Missey *et al.* [19], the impact of fuel stratification on the propagation of cryogenic fuel-lean flame above a liquid hydrogen pool was analyzed. They found that flame instabilities play a role in flame kernel development in the early stage. However, the impact of instabilities on long-term flame propagation and acceleration was not thoroughly discussed. For fuel-lean hydrogen/air flames at cryogenic temperatures, the combined effects of DLI and DTI may lead to even stronger flame acceleration, posing risks to the safe use of hydrogen. In the literature, there is a lack of quantitative analysis on the effects of DLI and DTI on the evolution and acceleration of cryogenic fuel-lean hydrogen/air flame, which inspires the present study.

There are several theoretical studies on linear instabilities development for planar flame [20, 21], circular expanding flame [22], and spherical expanding flame [23]. However, for fuel-lean hydrogen/air flames, Frouzakis *et al.* [24] have shown that linear theory fails to predict the dispersion relation. In addition, the non-linear evolution of wrinkled flames is more relevant to practical applications since linear evolution only lasts for a relatively short interval. Although analytical theory [25, 26] on the non-linear evolution of unstable flames has been developed, it cannot be readily applied to cryogenic flame evolution due to the strong assumption of weak thermal expansion. To account for realistic thermal expansion, a modified model in the context of hydrodynamic theory [27, 28] has been developed. However, the modified model requires numerical treatment, and the internal structure of the flame front is greatly simplified. Therefore, numerical research is still needed to study the evolution and acceleration of the fuel-lean hydrogen/air flames at cryogenic temperatures.

Various numerical studies in the literature have focused on the evolution of premixed hydrogen/air flames at ambient temperatures [29–34]. Berger *et al.* [15] investigated the effects of pressure, equivalence ratio, and temperature on premixed hydrogen/air flame instabilities in the linear stages. They found that intrinsic instabilities can be enhanced by decreasing the equivalence ratio and the temperature of the unburnt gas or by increasing the pressure. Later on, they studied the non-linear evolution of unstable hydrogen/air flames subjected to instabilities including DLI and DTI [31]. Their results showed that the instability development in the non-linear stage is affected by equivalence ratio, initial temperature, and pressure in the same manner as that in the linear stage in [15]. A recent study by Attili *et al.* [35] suggested that pressure can affect the development of DLI through different mechanisms. In addition, the contribution of DLI and DTI, as well as the synergistic interaction between DLI and DTI on flame evolution, was investigated numerically by Berger *et al.* [36]. However, none of the studies mentioned above covered the cryogenic temperature range. The impact of cryogenic temperatures on fuel-lean hydrogen/air flame evolution and accelerative propagation remains unclear. This motivates the present study, which focuses on the instability development of cryogenic fuel-lean hydrogen/air flames.

Given the background mentioned above, this study aims to investigate the fuel-lean hydrogen/air flame propagation subjected to intrinsic instabilities at cryogenic temperatures, focusing on the long-term non-linear evolution and acceleration associated with strong DLI and DTI. The paper is organized as

follows. Section 2 provides an overview of the numerical models and details on the setup. Then, Section 3 presents the simulation results and discusses various factors affecting the propagation and acceleration of fuel-lean flames. Finally, Section 4 summarizes the findings of this study.

2. Numerical model and methods

We consider premixed hydrogen/air flame propagation in a two-dimensional rectangular channel, as shown in Fig. 1. This configuration has been used to study flame instabilities [24, 29, 36]. The flame propagates from the right end to the left. Periodic boundary conditions are imposed on the top and bottom of the domain, while inflow and outflow boundary conditions are applied to the left and right boundaries, respectively. Note that periodic boundary conditions, rather than wall boundary conditions, are employed to prevent the flame quenching, which could otherwise affect the development of flame instabilities.

Figure 1: Schematic of the computational domain for the planar H_2/air flame propagating towards the left inlet.

We consider factors affecting the flame instabilities, including equivalence ratio ϕ, initial temperature T_0, and channel width h. Although the fuel-lean hydrogen/air mixtures with the equivalence ratio of ϕ=0.5 and initial temperatures of $T_0 = 100$ K and 300 K are the focus of this study, simulations with ϕ=1.0 and ϕ=2.5 are conducted to evaluate the effect of DLI alone, as shown in Table 1.

The channel width depends on the equivalence ratio and temperature of the mixture. The length of the computational domain is fixed to $L = 100\delta$, where δ is the flame thickness of the corresponding 1D premixed planar flame. It is determined by the maximum temperature gradient, i.e., $\delta = (T_b - T_0)/(dT/dx)_{max}$. Here T_b and T_0 are the temperatures of burned and

Table 1: Cases with different initial temperatures (T_0) and equivalence ratios (ϕ) considered in this study.

cases	$\phi = 0.5$	$\phi = 1$	$\phi = 2.5$
$T_0 = 100$ K	DLI&DTI	DLI	weak DLI
$T_0 = 300$ K	DLI&DTI	DLI	weak DLI

unburned gases, respectively. Cantera [37] is used to calculate 1D unstretched planar flame parameters, such as laminar flame speed S_L and flame thickness δ. The width of the computational domain varies by case, and a series of values are considered: h=4δ, 5δ, 6δ, 8δ, 10δ, 40δ, and 100δ. According to a previous study [30], for unstable hydrogen/air flames, a large domain ($h > 25\delta$) is necessary to ensure that the channel width does not constrain the development of instabilities. Note that the flame is stable for channels with $h < 4\delta$, and the flame front remains planar without wrinkling. Therefore, these channel widths, unaffected by flame instabilities, are not considered in the present study.

The domain is initialized by the corresponding 1D flame profile, and the flame front is located at $x = 90\delta$. The unburned gas velocity from the inlet is S_L. By imposing small sinusoidal perturbations on the flame front, the flame propagates towards the inlet due to the development of instabilities. As adopted in the previous study [24], here we also take the perturbation amplitude as $A(t = 0) = 0.001\delta$, and the wavelength λ is set to be the channel width ($\lambda = h$) for different cases. In the following section, unless otherwise specified, the length and time scales are normalized by δ and δ/S_L, respectively.

The low-Mach number solver, PeleLM [38], is used to solve the Navier-Stokes equations for multi-component reactive flow in the low-Mach number limit. The detailed chemical mechanism developed by Konnov [39] and the mixture-averaged transport model are considered in the simulations. This mechanism was used in previous studies [14, 16] to simulate cryogenic hydrogen/air flame propagation. It is also found that results are insensitive to cryogenic temperatures [40]. The Soret diffusion effect is neglected in the simulations as previous studies [41–43] have shown that it does not lead to qualitative change to hydrogen flames and that its importance appears nearly constant from $T_0 = 300$ K to 100 K [44]. To perform the simulation efficiently, adaptive mesh refinement is employed with a base grid size of $\Delta x = \delta/4$. The

reaction front is consistently resolved using a fine grid with a minimum size of $\Delta x = \delta/32$ throughout the simulation. This grid is fine enough to resolve the thin flame front and avoid numerical noise [24, 27], which was considered to be a major factor that affects the evolution of large-scale flames [45]. After a short period of linear evolution, the chaotic evolution in the non-linear stage happens, which will be analyzed and discussed in the following section.

3. Results and discussion

3.1. Linear evolution of the fuel-lean H_2/air flames

Due to the unstable nature of the fuel-lean hydrogen/air flame, initial perturbations imposed on the flame front grow exponentially in the linear stage. We first examine the dispersion relation in the preceding linear stage to better understand non-linear flame evolution. The numerical growth rate is calculated based on the rate of perturbation amplitude $A(t)$ [2, 15, 46], i.e.,

$$\omega^* = \frac{1}{A(t)}\frac{\mathrm{d}A(t)}{\mathrm{d}t} = \frac{\mathrm{d}\ln[(A(t)]}{\mathrm{d}t} \tag{1}$$

As mentioned above, the growth rate and wavenumber are normalized by corresponding 1D unstretched planar flame parameters, the normalized growth rate ω and wavenumber k are

$$\omega = \omega^*\delta/S_L, k = k^*\delta = 2\pi\delta/h \tag{2}$$

The dispersion relation for lean premixed hydrogen flames at $T_0 = 100$ K and 300 K is shown in Fig. 2. To compare with results in the literature, data for the case at ϕ=0.5 and $T_0 = 300$ K extracted from [24] are also plotted in Fig. 2. It is seen that results for $T_0 = 300$ K are close to the results in [24]. Considering the difference in chemical reaction mechanisms, good agreement is achieved between these results and the literature.

As shown in Fig. 2, the cryogenic condition significantly impacts flame instability development in the linear stage. The normalized growth rate ω increases greatly at cryogenic temperatures of $T_0 = 100$ K. The maximum normalized growth rate at $T_0 = 300$ K ($\omega = 1.2$) is much smaller than the maximum normalized growth rate at $T_0 = 100$ K ($\omega = 3.5$). As discussed in [15], a larger maximum growth rate implies stronger flame instability.

Therefore, the flame instability is greatly enhanced at cryogenic temperatures. Note that the flame instability in the non-linear stage is relevant to the maximum growth rate in the linear stage [15, 31]. Therefore, the cryogenic temperatures are expected to affect the non-linear evolution of unstable flame. On the other hand, for each normalized wavenumber k smaller than the cut-off wavenumber at which the growth rate is zero, ω for $T_0 = 100$ K is always larger than that for $T_0 = 300$ K, indicating that perturbations in the range of unstable wavenumber grow faster at cryogenic temperatures.

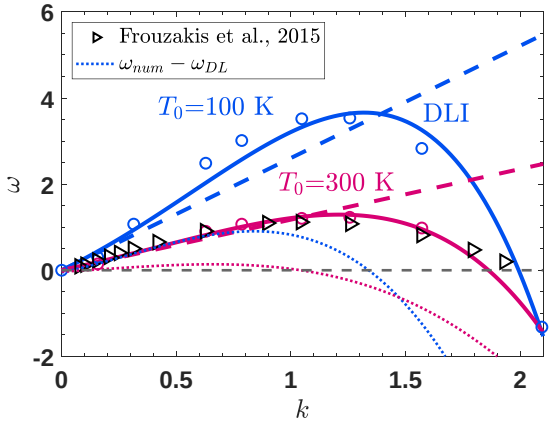

Figure 2: Dispersion relation for premixed H_2/air flames at ϕ=0.5, $T_0 = 100$ K and 300 K. The circles correspond to the numerical growth rate in this study. The solid curves are splines fitting these numerical growth rates according to Eq.(3). The black triangles refer to data extracted from [24]. Dashed lines are the theoretical growth rate of DLI. The dotted lines are the differences between the numerical and theoretical growth rates.

In the literature, the growth rate of lean flame is fitted by a fourth-order polynomial [15, 47] in the form:

$$\omega_{fit} = \omega_{DL} k + \Pi_2 k^2 - \Pi_4 k^4 \tag{3}$$

where ω_{DL} is the expression of the theoretical growth rate of DLI [10, 11, 29]:

$$\omega_{DL} = \frac{1}{\sigma + 1}(\sqrt{\sigma^3 + \sigma^2 - \sigma} - \sigma) \tag{4}$$

It is noted that in Eq.(3), there is no constraint on the coefficient Π_2, while the coefficient Π_4 must be positive to suppress the growth of short wavelength perturbations. The fitting coefficients according to Eq.(3) are listed in Table 2. To assess the individual effect of DLI, we also plot the

contribution of DLI for ambient and cryogenic flames based on Eq.(4), as denoted by the dashed lines in Fig. 2. It is seen that the growth rate of DLI, ω_{DL}, is larger at lower initial temperatures, indicating enhanced DLI at cryogenic temperatures.

On the other hand, the differences between numerical growth rate and theoretical growth rate are calculated and plotted in Fig. 2 to evaluate the contribution of DTI, as shown by the dotted lines. It is found that the growth rate due to DTI is also larger at lower initial temperatures. Additionally, in Table 2 the coefficient Π_2 for $T_0 = 100$ K is much larger than that for $T_0 = 300$ K. Since Π_2 is relevant to the effect of DTI, this also shows that DTI is enhanced due to the cryogenic conditions. Therefore, at cryogenic temperatures, not only is DLI enhanced, but DTI is also enhanced.

Table 2: Comparison of fitting coefficients for $T_0 = 100$ K and 300 K.

case	ω_{DL}	Π_2	Π_4
$T_0 = 100$ K	2.61	1.25	0.64
$T_0 = 300$ K	1.18	0.31	0.27

Although this dispersion relation is derived from the linear stage of flame evolution, it provides a reasonable estimate for the instability in the non-linear stage, as suggested by [15, 31]. Therefore, it is expected that in the non-linear stage, both DLI and DTI will also be greatly enhanced at cryogenic conditions for the fuel-lean premixed hydrogen/air flame.

3.2. Non-linear evolution of flame front propagation

The linear stage only lasts for a short interval. After a quick transition, the unstable flame evolution changes from the linear to the non-linear stage, characterized by complicated long-term dynamics of cellular structure evolution, including cell splitting, cell merging, and lateral movement [29]. Figure 3 shows the evolution of the lean flame (ϕ=0.5) front in the channel of $h = 10\delta$ for $T_0 = 100$ K and $T_0 = 300$ K. As flame instabilities develop, the flame surface area increases, and the flame propagates towards the unburnt gas on the left side. It is found that the perturbed sinusoidal flame quickly transitions to the non-linear evolution stage with two cusps on the front. During the flame propagation process, the shape of the flame front changes occasionally. For $T_0 = 100$ K shown in Fig. 3(a), the depth of the

two cusps is different after the planar flame changes to the two-cusp regime. The two-cusp flame front rapidly evolves to the single-cusp front at around x/δ=75. Then, the flame propagates forwards in this single-cusp regime for a long time with lateral movement. During this process, a double-cusp flame front appears occasionally with a relatively short lifetime.

The evolution of the ambient flame at $T_0 = 300$ K is different. As shown in Fig. 3(b), the flame shape changes from the two-cusp regime to the single-cusp regime at around x/δ=60. This structure lasts a short interval, then transitions to the two-cusp regime at around x/δ=58. However, this regime is unstable, and it reverts to the single-cusp regime. Finally, the flame moves towards the inlet in a single-cusp regime. The comparison between $T_0 = 100$ K and $T_0 = 300$ K demonstrates that the lateral movement is more pronounced, and the cusp is deeper for the cryogenic flame, which is thereby more unstable.

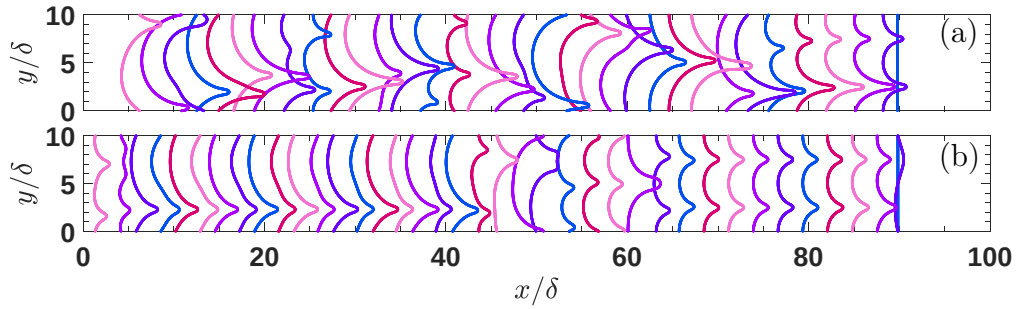

Figure 3: Temporal evolution of flame front propagating in a channel with $h = 10\delta$ for (a) $T_0 = 100$ K, ϕ=0.5, (b) $T_0 = 300$ K, ϕ=0.5. The flame propagates from the right to the left.

The flame front evolution for the stoichiometric case (ϕ=1) is shown in Fig. 4. It is noted that for the hydrogen/air mixture at ϕ=1, the effective Lewis number is slightly larger than unity, i.e., $Le_{eff} > 1$. Therefore, the flame is diffusional-thermally stable, and the primary factor affecting flame front evolution is DLI. It is seen that without DTI, the non-linear evolution of the hydrogen/air flame exhibits a relatively simple structure at both ambient and cryogenic temperatures. The flame propagates to the left side in a stable single-cusp regime without cell splitting or merging processes. In addition, the position of the single cusp on the flame front is almost the same at different instants, i.e., the cusp stays at around y/δ=7 without lateral movement. This indicates that DLI plays a limited role in the non-linear evolution of the

flame front. Combined with previous lean flame results, dynamics of non-linear evolution, including cell splitting, cell merging, and lateral movement, are more associated with the DTI.

Nevertheless, the intensity of flame instability is different for $T_0 = 100$ K and $T_0 = 300$ K. Comparison between Figs. 4(a) and (b) shows that the normalized cell depth is larger at a cryogenic temperature of $T_0 = 100$ K. This demonstrates that DLI is enhanced at cryogenic temperatures in the non-linear stage.

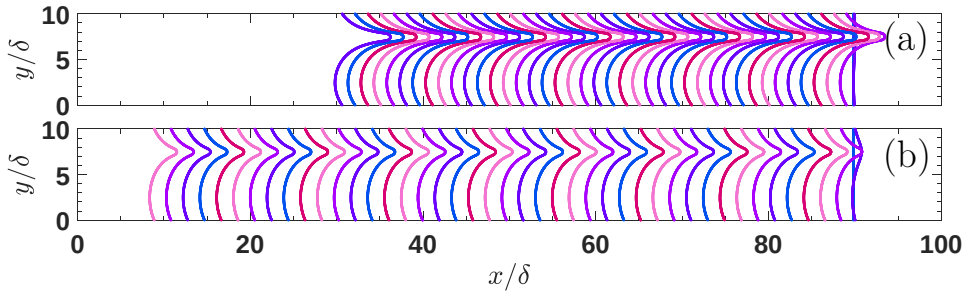

Figure 4: Temporal evolution of flame front propagating in a channel with $h = 10\delta$ for (a) $T_0 = 100$ K, ϕ=1, (b) $T_0 = 300$ K, ϕ=1. The flame propagates from the right to the left.

Simulations were also performed on the fuel-rich hydrogen/air mixture with ϕ=2.5. The flame evolution in the non-linear stage is similar to the stoichiometric case shown in Fig. 4. The results for ϕ=2.5 are not shown here to avoid duplication. The primary difference between ambient and cryogenic flames is the normalized cusp depth, which is larger for $T_0 = 100$ K, indicating stronger DLI at lower temperatures.

As mentioned above, the channel width may significantly affect the flame evolution. To study this effect, Fig. 5 shows the fuel-lean cryogenic flame ($T_0 = 100$ K, ϕ=0.5) propagation in channels with different widths. Note that the evolution of the flame front for $h = 10\delta$ is shown in Fig. 3 and is not repeated in Fig. 5 to avoid redundancy. As the channel width increases from $h = 4\delta$ to $h = 10\delta$, the non-linear evolution of the flame front exhibits distinguishing regimes: For $h = 4\delta$, the regime is a stable single-cusp flame front, with one small cusp located at around y/δ=3. For $h = 5\delta$, the flame front is a single-cusp regime with lateral movement. When the channel width increases to $h = 6\delta$, the flame regime changes again: the flame propagates towards the unburned gas in a complex regime, in which single-cusp and two-cusp alternately appear on the flame front. By further increasing to $h = 8\delta$,

the flame regime is a stable double-cusp regime in which two cusps on the flame front with a fixed position at y/δ=2 and y/δ=6. Interestingly, the flame front shape for $h = 8\delta$ seems to be mirrored from that for $h = 4\delta$. The quasi-steady propagation regime (stable single-cusp and double-cusp) observed in cases with $h = 4\delta$ and 8δ may be related to the critical wavenumber (k_m) associated with the maximum normalized growth rate. According to the results in Fig. 2, $k_m \approx 1.32$, corresponding to a critical wavelength of $\lambda_m \approx 4.7\delta$. The channel widths for the quasi-steady propagation regime are close to, but slightly smaller than, the integer multiples of λ_m. This observation is also consistent with the results in the previous study [24]. When the channel width is $h = 10\delta$, as shown in Fig. 3(a), the flame propagation regime is alternative single-cusp and double-cusp. Therefore, the non-linear evolution of the flame front is very sensitive to the change in channel width.

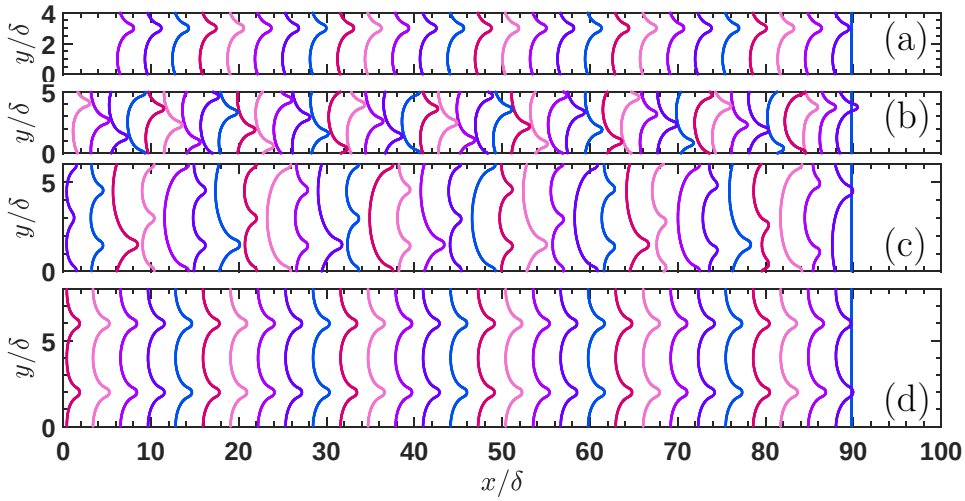

Figure 5: Temporal evolution of fuel-lean cryogenic flame ($T_0 = 100$ K and ϕ=0.5.) front propagating in channels with different widths: (a) $h = 4\delta$, (b) $h = 5\delta$, (c) $h = 6\delta$, and (d) $h = 8\delta$. The flame propagates from the right to the left.

Previous studies [30, 36, 48] have shown that the channel width strongly influences the flame structure. The "flame finger" structure [36] cannot be observed when the channel width is too small. It is found that the channel width larger than 25δ is proper for the evolution of flame finger structure. As shown in Fig. 6(a), one flame finger structure can be observed for $h = 20\delta$. Moreover, the flame finger is smooth, and small wrinkles do not appear on the flame branches that compose the flame finger structure. When the channel

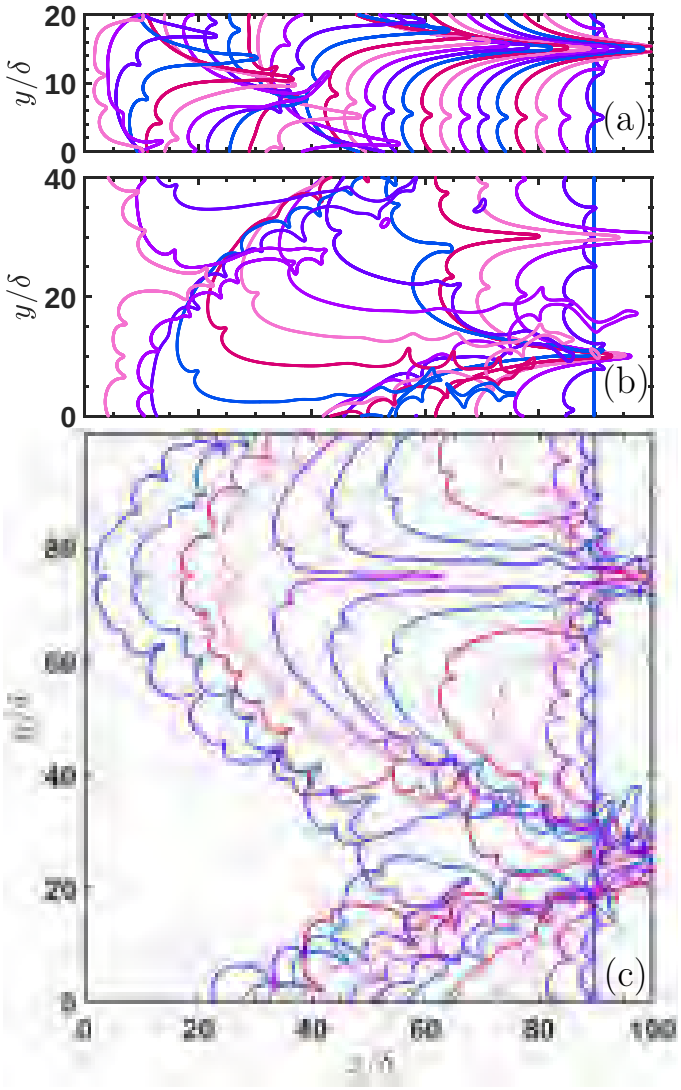

Figure 6: Temporal evolution of flame front propagating in channels with different widths (a)$h = 20\delta$, (b) $h = 40\delta$, and (c)$h = 100\delta$ for $T_0 = 100$ K and ϕ=0.5. The flame propagates from the right to the left.

width increases to $h = 40\delta$, as shown in Fig. 6(b), a flame finger structure with small wrinkles superimposed on its branches is observed. This structure exhibits distinct lateral movement. In addition, isolated flame pockets can be observed in the late stage due to the collision of wrinkled flame segments. The results for $h = 100\delta$ are shown in Fig. 6(c). After transitioning to the

non-linear stage, small flame finger structures with lateral movement can merge into a large flame finger. There are many small wrinkles with different length scales on the branches of the flame finger. The flame front is wrinkled and accelerated as it propagates towards the unburnt gas.

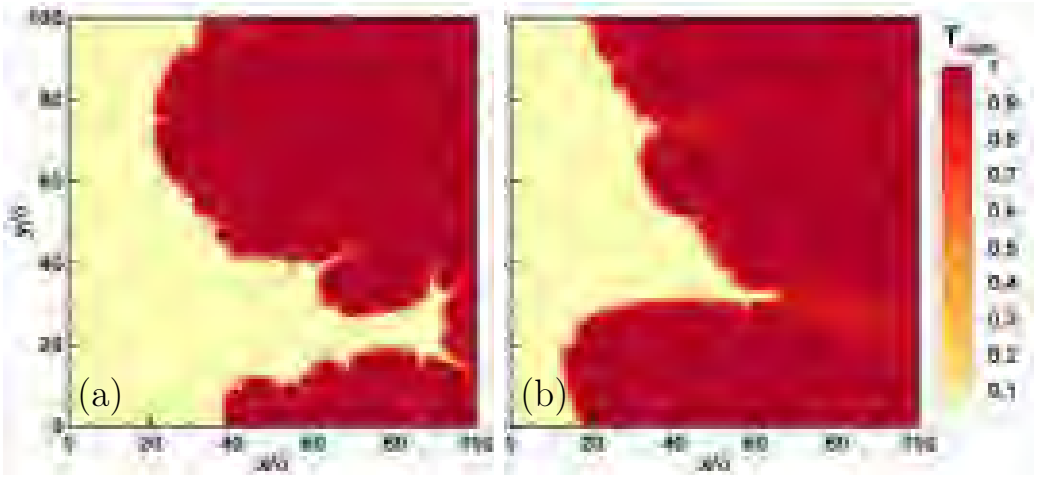

Figure 7: Contours of normalized temperature (T_{norm}) for (a) $T_0 = 100$ K at $t = 20.8$ and (b) $T_0 = 300$ K at $t = 92$. The channel width is $h = 100\delta$.

The contours of normalized temperature ($T_{norm} = (T - T_0)/(T_b - T_0)$) at the instant when a cellular structure is fully developed are shown in Fig. 7. It is seen that the cryogenic flame front is more wrinkled compared to the ambient flame. In addition, the intense wrinkling of the cryogenic flame forms a deep channel containing unburnt gas between large flame finger structures. The subsequent combustion of the unburnt gas within the deep channel produces a sharp reduction in the flame surface area. As a result, the surface area of the cryogenic flame can vary significantly during propagation. Consistent with previous study [49], super-adiabatic temperature phenomena are observed for both fuel-lean flames, with $T_{norm,max} = 1.1$ for $T_0 = 100$ K and $T_{norm,max} = 1.05$ for $T_0 = 300$ K. Since the super-adiabatic temperature phenomena are associated with the imbalance between thermal and species diffusion, the larger super-adiabatic temperature at cryogenic conditions indicates that DTI is more pronounced at lower temperatures.

It is clear that the alternating appearance of single-cusp and double-cusp flame fronts and the evolution of flame finger structures in fuel-lean premixed hydrogen/air flames are closely related to long-term dynamics, including cell

splitting, cell merging, and lateral movement [29]. To better understand the flame evolution, their mechanisms are analyzed in the following subsection.

3.3. Long-term flame dynamics

To investigate the mechanism for cellular structure splitting and merging, the evolution of the heat release rate (HRR) contour and the corresponding flow field near the flame front is considered for the fuel-lean cryogenic case ($T_0 = 100$ K, ϕ=0.5, $h = 10\delta$). The flame front is defined as the iso-contour line of the mass fraction of H_2O, which corresponds to the maximum temperature gradient of the 1D unstretched planar flame. Streamlines near the flame front are superimposed on the HRR contour to interpret the cell splitting and merging process in Figs. 8(1a-1c) and 8(2a-2c), respectively. Figure 9 shows the profiles of flow speed in the x direction U_x, local heat release rate q, density-weighted displacement speed S_d^*, stretch rate K along the flame front and the flame front position x as functions of y for several instants during the cell splitting and merging processes. It is noted that in Figs. 9(1e) and (2e) the flow direction in the unburnt region is from bottom to top and all parameters except q are normalized.

The splitting process of cellular structure is relevant to the interactions between the flame stretch, local reactivity, and flow. In Fig. 8(1a) at t=56.4, the flame cell is relatively smooth, and a large cusp is located at around y/δ=2. A streamline focusing phenomenon is observed near the cusp. As shown in Fig. 9(1a), the unburnt gas speed ahead of the cusp is larger than that near the convex segment of the cell. This is a feature of DLI due to the interaction between the flame front and the flow near it [11, 20]. Gas expansion across the flame front induces flow acceleration, which enhances the flame front wrinkling and leads to a deeper cusp. In the middle of the large cell at around y/δ=8, the flame stretch rate becomes negative, and the HRR is relatively small compared with the two flame branches near it, which can be seen in Figs. 9(1b) and (1d) at t=56.4. Therefore, a small concave segment towards the unburnt gas is formed, indicating the birth of a new cusp. As this concave segment evolves in the flow, its depth increases due to the interaction between flow and flame front, as shown in Figs. 8(1b) and 9(1a-1e). This process is relevant to the development of DLI. Therefore, the streamline focusing phenomenon becomes significant near the new cusp at around y/δ=8. In Figs. 8(1c) and 9(1e), this new cusp forms with considerable depth. Note that the interaction between flame stretch and chemistry also plays an important role in the cell splitting process since the

cusp deepening process is accompanied by a change in curvature and flame stretch rate that affects the chemical reaction through Lewis number effect, as shown in Figs. 9(1b) and (1d). In summary, the complex interactions between flow, flame stretch, and chemistry lead to the splitting of flame cells and the formation of a new cusp on the flame front.

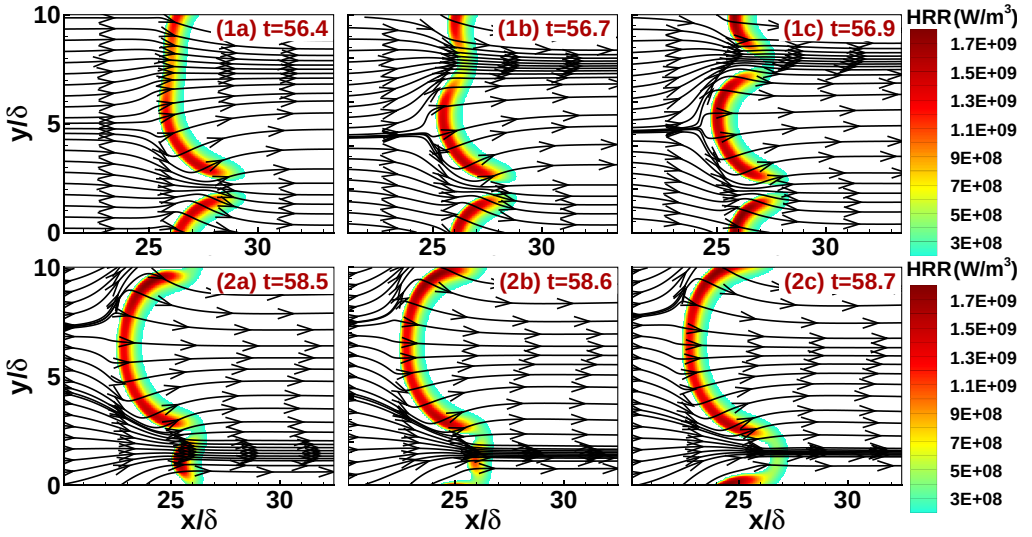

Figure 8: Evolution of heat release rate contour superimposed by streamlines near the occurrence of cell splitting (1a-1c) and cell merging event (2a-2c) for T_0 = 100 K and ϕ=0.5. The channel width is $h = 10\delta$.

The cell merging process is shown in Figs. 8(2a-2c) and 9(2a-2e). Note that a periodic boundary condition is imposed in the y direction. At t=58.5 in Figs. 8(2a) and 9(1e), the flame front consists of two convex cells with different length-scales: a large cell within the range of $2.5 \leq y/\delta \leq 10$ and a small cell within $0 \leq y/\delta \leq 2.5$. These two cells are connected by two cusps between them. Since the HRR on the larger cell is not uniform, the propagation speed is different along the flame front of the large cell. Specifically, the HRR is larger on two branches of the large cell near the cusps and smaller in the middle of the cell. This can be observed in Figs. 8(2a-2c) and 9(2b). Therefore, the large cell tends to expand in the lateral direction (y direction), which narrows the channel ahead of the small cell, as shown in Figs. 8(2b) and 9(2a-2e). Flow focusing also contributes to the increase in cusp depth. The narrow channel ahead of the small cell acts like a 'cusp', and therefore, the flow speed in the 'cusp' ($0 \leq y/\delta \leq 2.5$) increases as the

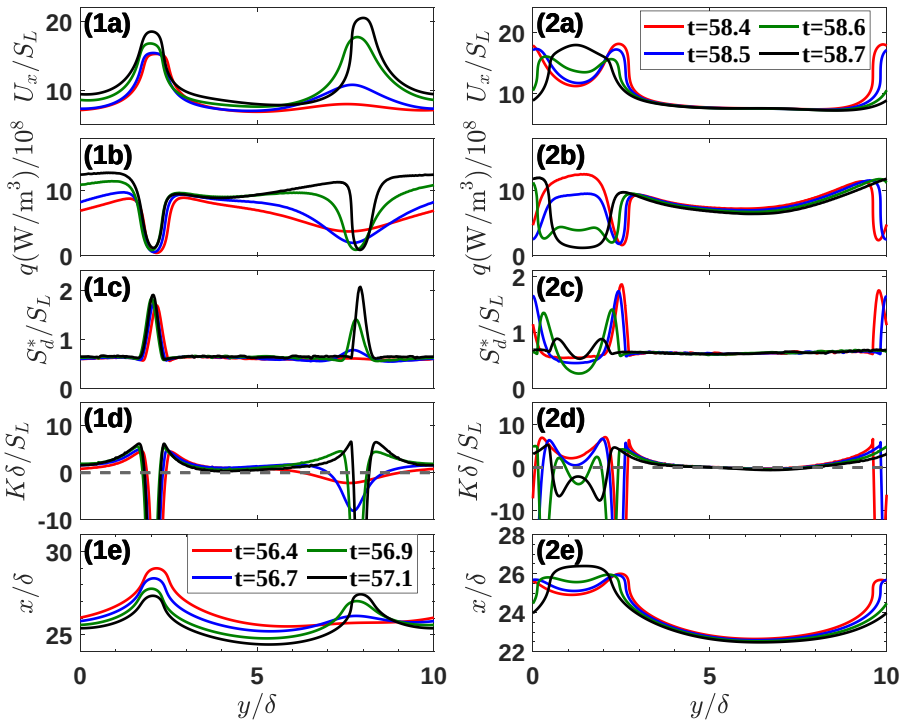

Figure 9: Temporal evolution of profiles for flow speed, U_x, heat release rate, q, density-weighted displacement speed, S_d^*, stretch rate, K, and the flame front position, x, along the flame front during cell splitting (1a-1e) and cell merging process (2a-2e).

large cell expands, as shown in Figs. 8(2b) and 9(2a). Due to the increased flow speed, the small flame cell cannot propagate towards the unburnt gas on the left. Gradually, it is pushed back by the strong flow. As a result, the small cell becomes flat (see Fig. 9(2e)). Since the differential diffusion effect is strong for this negatively stretched flame segment (see in Fig. 9(2d)), the HRR of the smaller cell also decreases gradually during this process, which can be seen in Fig. 9(2b). Finally, as shown in Fig. 8(2c), the small cell disappears, implying the completion of the cell merging process. Therefore, the cell merging is also associated with the interaction between flow, flame stretch, and chemical reactions.

In addition, Fig. 9(1b) also explains the mechanism for the lateral movement of cusps. At t=56.9 (green line), there is a manifest difference in heat release rate between the two flame branches forming the cusp at y/δ=2. Affected by this, the flame propagation speeds are also different. Therefore, the

strong flame branch near y/δ=1 pushes the weak flame branch near y/δ=3, leading to the lateral movement of the cusp towards the y-axis direction. Therefore, the cusp moves to the right from t=56.9 to t=57.1 (black line), which can be seen from Fig. 9(1e). As mentioned above, the HRR distribution is affected by the cell splitting and merging processes. Therefore, lateral movement is frequently observed for flames in the regime of alternative appearance of single-cusp and double-cusp, as can be observed in Figs. 3, 5(b), 5(c) and 6.

In summary, strong interaction among flow, flame stretch, and chemical reactions (heat release) plays a primary role in the cell splitting and merging processes. Therefore, the mechanisms of the chaotic evolution of the fuel-lean flame front are relevant to the 'flow-stretch-chemistry' interaction.

3.4. Cellular flame structure

In order to interpret the effect of cryogenic temperatures on the local flame structure, the joint distribution of progress variable (PV) and the normalized reaction rate of hydrogen are analyzed. The progress variable is defined as

$$PV(Y(\mathrm{H_2})) = 1 - \frac{Y(\mathrm{H_2}) - Y_b(\mathrm{H_2})}{Y_u(\mathrm{H_2}) - Y_b(\mathrm{H_2})} \tag{5}$$

where $Y(\mathrm{H_2})$ is the mass fraction of $\mathrm{H_2}$, $Y_u(\mathrm{H_2})$ and $Y_b(\mathrm{H_2})$ are the mass fraction of $\mathrm{H_2}$ in the unburnt and burned gas, respectively.

The joint distribution, conditional average and 1D unstretched planar flame solution of progress variable and corresponding source term for case $h = 10\delta$ are shown in Fig. 10. It is seen that for the fuel-lean flames, the conditional average of source term is much higher than the 1D unstretched flame solution. On the other hand, in Fig. 10(c), the cryogenic flame at ϕ=1, the conditional average of source term is close to the 1D unstretched planar flame solution, indicating that the effects of DLI on local flame structure and the enhancement in reaction rate are negligible. Comparison in Fig. 10 demonstrates that DTI of fuel-lean flames has a significant impact on the local reaction rate enhancement. Therefore, DLI accelerates flame propagation mainly through the increase in the flame surface area, while DTI can lead to flame acceleration through both an increase in the flame surface area and local reaction rate enhancement. Furthermore, compared to the ambient flame at T_0 = 300 K and ϕ=0.5, the cryogenic flame at ϕ=0.5 exhibits a larger normalized conditional average of the source term, which demonstrates that

at a lower temperature, the DTI has a stronger influence on local reaction rate enhancement.

To assess the effect of channel width on flame propagation, the joint distribution of the progress variable and the corresponding source term for $h = 100\delta$ is shown in Fig. 11. It is seen that the normalized conditional averages of the source term do not change significantly from cases $h = 10\delta$ shown in Fig. 10. Therefore, increasing the channel width from $h = 10\delta$ to $h = 100\delta$ has a limited effect on the local reaction rate enhancement for the fuel-lean flames considered in this work.

3.5. Flame acceleration

Strong DLI and DTI can greatly enhance the flame front wrinkling, accelerating flame propagation. An approximate measure of the flame speed for the wrinkled flame is consumption speed, S_c, defined as in [31],

$$S_c = \frac{1}{\rho_u(Y_u(\mathrm{H_2}) - Y(\mathrm{H_2})) \cdot A_0} \int \dot{\omega} dx dy \tag{6}$$

where $\dot{\omega}$ is the net consumption rate of H_2, ρ_u the unburned gas density, $Y_u(H_2)$ the mass fraction of H_2 in the unburned gas, A_0 the flame surface area at t=0, i.e., $A_0 = h$. Generally, flame instabilities can affect overall flame speed through two mechanisms: flame surface area increase due to flame wrinkling and local flame speed change related to flame stretch [36, 50]. To quantify their individual effect, S_c is decomposed into the production of flame surface area increase A/A_0 and stretch factor I,

$$S_c/S_L = I \cdot (A/A_0) \tag{7}$$

where A is the surface area of the wrinkled flame front. It is noted that the fuel-lean flame surface is defined as the iso-contour line of $PV(Y(H_2))$=0.9 [49]. This definition leads to reasonable results for the flame surface area, especially for the fuel-lean flame, which is prone to strong DTI. For stoichiometric or fuel-rich cases, the iso-contour line of water mass fraction ($Y(H_2O)$) corresponding to the maximum temperature gradient of the 1D unstretched planar flame is selected to the calculated flame surface area, as the differential diffusion effect could lead to locally fuel-rich mixture [31]. The stretch factor measures the effect of local reactivity on the consumption speed. If $I > 1$, the effect of flame stretch enhances the consumption of fuel (local reaction rates) and vice versa.

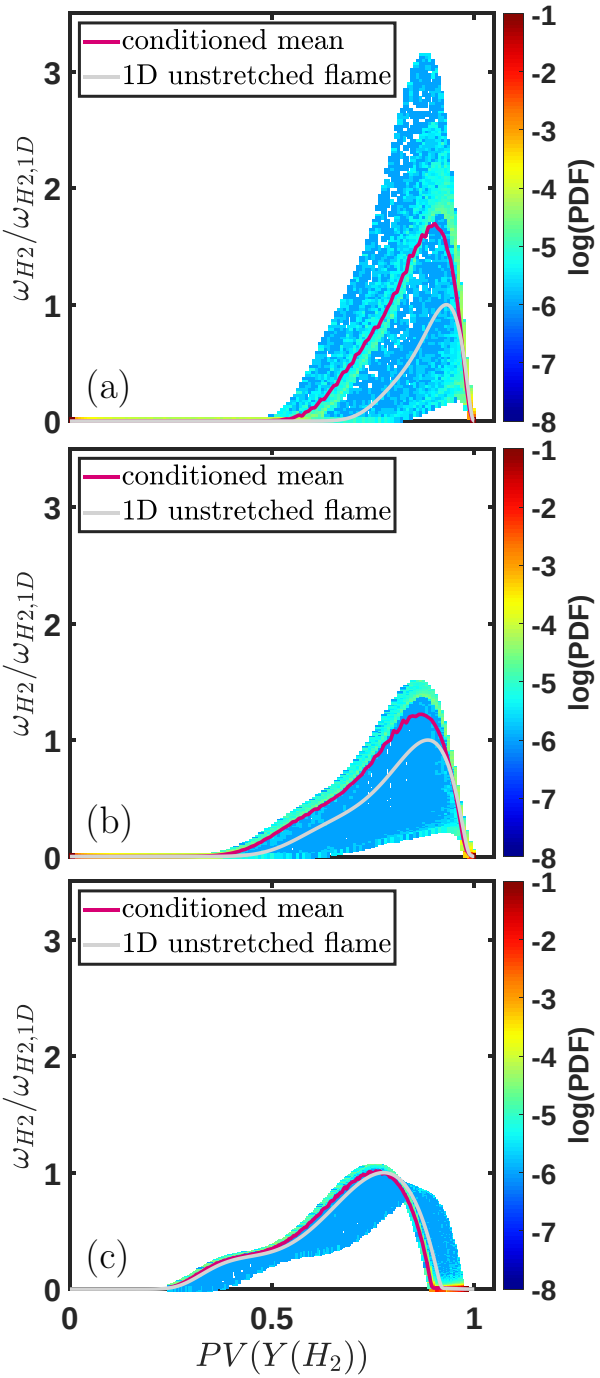

Figure 10: Joint distribution, conditional average (red line) and 1D unstretched flame solution (grey line) of the progress variable $PV(Y(\mathrm{H_2}))$ and the normalized source term of $PV(Y(\mathrm{H_2}))$ for (a)T_0 = 100 K, ϕ=0.5, (b) T_0 = 300 K, ϕ=0.5, and (c) T_0 = 100 K, ϕ=1. The channel width is $h = 10\delta$.

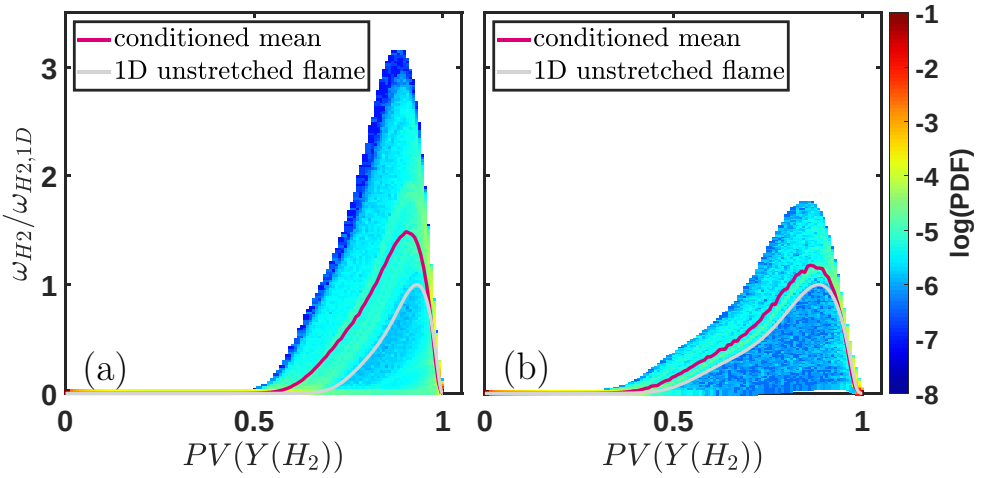

Figure 11: Joint distribution, conditional average (red line) and 1D unstretched flame solution (grey line) of the progress variable $PV(Y(\mathrm{H_2}))$ and the normalized source term of $PV(Y(\mathrm{H_2}))$ for (a)$T_0 = 100$ K, ϕ=0.5 and (b) $T_0 = 300$ K, ϕ=0.5. The channel width is $h = 100\delta$.

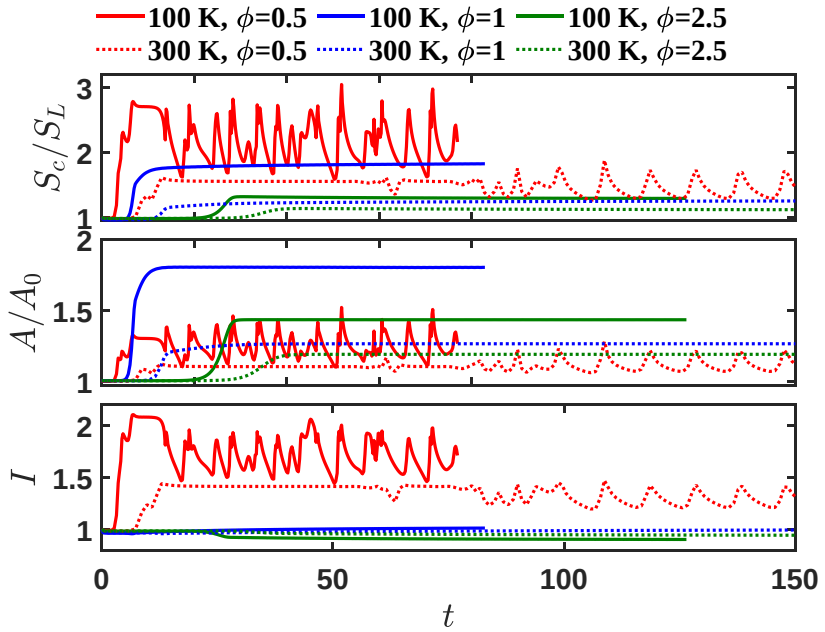

Figure 12: Evolution of the normalized consumption speed S_c/S_L, flame surface area increase A/A_0 and stretch factor I for case $T_0 = 100$ K and ϕ=0.5, $h = 10\delta$.

The effect of equivalence ratio and cryogenic temperatures on flame evolution for $h = 10\delta$ is shown in Fig.12. It is found that the consumption speed oscillation is only observed for $\phi = 0.5$ with strong DTI. This result is reasonable since the chaotic evolution of cellular structure originates from DTI. On the other hand, the acceleration of fuel-lean cryogenic flame is the most pronounced, highlighting that the combined effects of both DLI and DTI have a significant influence on flame acceleration. Further analyses shown in Figs. 12(b) and (c) demonstrate that the acceleration results from enhancement in both A/A_0 and I. The primary contribution is from the increase in I. This shows that DTI is the dominant factor in fuel-lean flame acceleration, consistent with the previous study [36]. In addition, pure DLI also leads to intense flame acceleration, which can be seen in the cryogenic and ambient cases at $\phi = 1$. For fuel-rich flames, flame acceleration is greatly suppressed, with S_c/S_L close to 1. It is clear that for $\phi \geq 1$, the acceleration is purely caused by an increase in A/A_0. The local reaction rate is not enhanced by DLI, which is consistent with the results shown in Fig. 10(c).

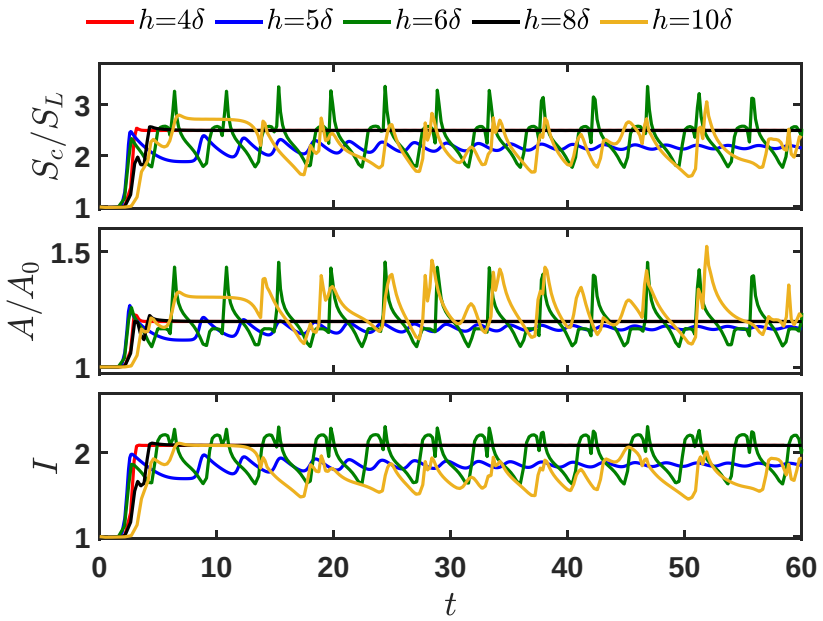

Figure 13: Evolution of the normalized consumption speed S_c/S_L, flame surface area increase A/A_0 and stretch factor I for case $T_0 = 100$ K and ϕ=0.5 in domain with different widths h.

Figure 13 shows the effect of channel width ($h \leq 10\delta$) on the flame

acceleration in the fuel-lean mixture at $T_0 = 100$ K. The flame speed changes periodically due to chaotic cell evolution. The time period of oscillations is affected by both the channel width and the lateral movement speed. However, the lateral movement speed is complex and can be affected by many factors, such as the nonlinear behavior of the flame front, the Lewis number and the temperature distribution along the flame front [51]. Deriving an analytical expression for the oscillation period is beyond the scope of this work and warrants further investigation. In addition, the flame speed enhancement, S_c/S_L, is larger than 1.5 for all channel widths considered. Both A/A_0 and I contribute to the flame acceleration. Moreover, Fig. 13 shows that the stretch factor I oscillates around $I = 2.0$ with a lower bound of $I > 1.5$, while A/A_0 fluctuates around $A/A_0 = 1.2$ with an upper bound of $A/A_0 < 1.5$. Since I is only relevant to the DTI and the DTI also contributes to A/A_0, it can be concluded that the DTI plays a dominant role in fuel-lean flame propagation. Previous studies [36, 50] have shown that DLI can enhance the development of DTI. Therefore, DLI may also play a role in flame acceleration through a direct mechanism of increasing flame surface area or through an indirect mechanism of promoting DTI. It is worth noting that the dependence of S_c/S_L, A/A_0 and I on h is sensitive, which is caused by the chaotic evolution of the flame front under strong DTI and DLI. Therefore, channel width has a significant effect on flame evolution regimes and thereby flame acceleration, especially for narrow channels.

Table 3: The mean values of normalized consumption speed S_c/S_L, flame surface area increase A/A_0, ans stretch factor I for fuel-lean hydrogen/air flame at $T_0 = 100$ K and 300 K. The channel width is $h = 100\delta$.

case	S_c/S_L	A/A_0	I
$T_0 = 100$ K	4.25	1.95	2.17
$T_0 = 300$ K	2.04	1.40	1.45

As mentioned above, a large domain is necessary to obtain geometry-independent results. For flame propagation in wide channels, the results are shown in Fig. 14. Based on the data after the cellular structure is fully developed in the wide channel of $h = 100\delta$, the domain-independent mean values of S_c/S_L, A/A_0, and I for fuel-lean hydrogen/air flames at $T_0 = 100$ K and 300 K are calculated and listed in Table 3. Compared to $T_0 = 300$ K, the larger S_c/S_L at $T_0 = 100$ K results from the increase in both A/A_0 and I,

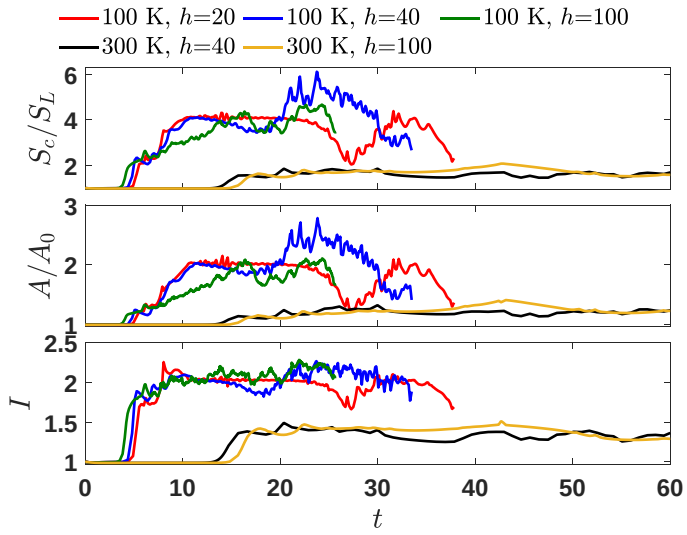

Figure 14: Evolution of the normalized consumption speed S_c/S_L, flame surface area increase A/A_0 and stretch factor I for ϕ=0.5 in domain with different widths and initial temperatures.

which demonstrates that both DLI and DTI are enhanced under cryogenic conditions. Since the values of I are larger than A/A_0, the DTI has a greater contribution to the flame acceleration than the DLI. It is noted that the mean values in Table 3 for the cryogenic flame are calculated during the later stage of flame propagation, when most of the flame segments are contained within the computational domain. A small portion of flame segments extending beyond the domain may lead to slightly underestimated mean values; however, this does not affect the main conclusions.

Comparison between Figs. 13 and 14 shows that the periodic oscillation phenomena disappear when the channel width is large. Only small spikes appear on the evolution of consumption speed in Fig. 14. This is reasonable since the cellular flame front evolution is more violent without the confinement of channel width. Additionally, the large oscillations observed in Fig. 14 are relevant to the flame segments extending beyond the computational domain, which causes a pronounced reduction in flame surface area and flame consumption speed. Compared to small channels shown in Fig. 13, the value of A/A_0 for a cryogenic flame increases to around $A/A_0 \approx 1.95$, while the stretch factor I does not increase significantly. Therefore, a small channel width can suppress the development of flame instabilities through the flame

surface area, resulting in weaker flame acceleration. On the other hand, the stretch factor I is less sensitive to the channel width, which agrees well with the analysis in the previous section.

An interesting observation is the large value of $S_c/S_L \approx 6$ for $h = 40\delta$ in Fig. 14(a) and 14(b) shows that this large value is associated with an increase in flame surface area, resulting from the formation of a very deep cusp during the flame propagation, as shown in Fig. 6(b). Compared to the case with $h = 100\delta$, a smaller channel width of $h = 40\delta$ enhances the flame acceleration. Therefore, a smaller channel width does not always suppress the flame wrinkling and flame acceleration. This also indicates that channel width has a great impact on cellular flame evolution and acceleration.

4. Conclusions

The evolution and acceleration of fuel-lean hydrogen/air flames at ambient and cryogenic temperatures (300 K and 100 K) are studied by a series of two-dimensional simulations incorporating detailed chemistry and transport models. The analysis reveals that cryogenic temperatures significantly enhance both Darrieus-Landau instability (DLI) and diffusional-thermal instability (DLI) of fuel-lean hydrogen/air flames. In the linear stage, the growth rates of both DLI and DTI are found to increase significantly at cryogenic temperatures. The non-linear stage of cellular flame evolution exhibits chaotic characteristics influenced by unburned gas temperature and channel width, with DTI emerging as the primary driver of this chaotic evolution. Long-term dynamics of cellular structures, including cell splitting, cell merging, and lateral movement, are observed and interpreted for fuel-lean hydrogen/air flames. It is found that cell splitting and merging are mainly caused by the flow-stretch-chemistry interaction. The unbalanced heat release rate on two branches of the cusp can induce the lateral movement of cusps. In the absence of DTI, the flame propagates in a single-cusp regime without cell splitting, merging, or lateral movement due to a relatively weak stretch-chemistry interaction.

Flame structure analysis reveals a significant enhancement of local reaction rates in lean hydrogen/air flames under cryogenic conditions. For diffusive-thermally stable hydrogen/air flames with $\phi = 1$, the cryogenic temperature has a negligible effect on the local reaction rate. The pronounced acceleration of fuel-lean cryogenic flames stems from the simultaneous enhancement of flame surface area and stretch factor, reflecting the combined

influence of DLI and DTI. While both instabilities contribute to flame acceleration, DTI emerges as the dominant mechanism, with DLI providing secondary enhancement. The flame evolution demonstrates particular sensitivity to channel geometry when the width $h < 10\delta$: minor width variations can substantially alter the evolution of flame consumption speed. Further analysis indicates that channel width influences flame behavior primarily by constraining the flame surface area, while local reaction rates remain largely independent of geometric constraints.

In this study, the Soret diffusion is not considered. In previous study [52], the Soret diffusion effect was examined at elevated temperatures. It would be interesting to quantify the influence of the Soret diffusion at cryogenic temperatures in future studies. Our study employs two-dimensional simulations, which capture important aspects of flame dynamics but have inherent limitations. In real-world applications, flames propagate three-dimensionally, potentially exhibiting additional instability mechanisms that could enhance flame front wrinkling and acceleration beyond what we observe in two dimensions. Introducing the third dimension may reveal new patterns of flame evolution and more complex interactions between DLI and DTI. Future investigations using three-dimensional simulations in large computational domains would complement our current findings and provide a more complete understanding of flame behavior under cryogenic conditions.

5. Declaration of competing interest

The authors declare that they have no known competing financial interests or personal relationships that could have appeared to influence the work reported in this paper.

6. Acknowledgments

This work was funded by the National Natural Science Foundation of China (No. 52425604). This work was supported by funding from the Engineering and Physical Sciences Research Council IAA (Grant number EP/R511742/1). Dr. Linlin Yang gratefully acknowledges the financial support from the John Fell Oxford University Press Research Fund (0016719). Dr. Fang acknowledges the financial support provided by the NSERC and Alberta Innovate HCOE2 program. We also thank Dr. Hannes Böttler at the Technical University of Darmstadt for helpful discussions.

References

[1] Z. Abdin, A. Zafaranloo, A. Rafiee, W. Mérida, W. Lipiński, K. R. Khalilpour, Hydrogen as an energy vector, Renew. Sustain. Energy Rev. 120 (2020) 109620.

[2] T. Lehmann, L. Berger, T. L. Howarth, M. Gauding, S. Girhe, B. B. Dally, H. Pitsch, Comprehensive linear stability analysis for intrinsic instabilities in premixed ammonia/hydrogen/air flames, Combust. Flame 273 (2025) 113927.

[3] M. Aziz, Liquid Hydrogen: A Review on Liquefaction, Storage, Transportation, and Safety, Energies 14 (2021) 5917.

[4] G. Tretola, L. Shen, F. Leach, K. Vogiatzaki, Mixing and Warming Characterisation of Cryogenic Hydrogen Jets Through Proper Orthogonal Decomposition, in: ASME 2024 ICE Forward Conference, American Society of Mechanical Engineers, San Antonio, Texas, USA, 2024, p. V001T06A012.

[5] D. Yu, Z. Chen, Premixed flame ignition: Theoretical development, Prog. Energy Combust. Sci. 104 (2024) 101174.

[6] S. Lai, S. Tang, C. Xu, N. Sekularac, X. Fang, Computational diagnostics for flame acceleration and transition to detonation in a hydrogen/air mixture, Combust. Flame 258 (2023) 113054.

[7] M. Kuznetsov, A. Denkevits, A. Veser, A. Friedrich, Flame propagation regimes and critical conditions for flame acceleration and detonation transition for hydrogen-air mixtures at cryogenic temperatures, Int. J. Hydrog. Energy 47 (2022) 30743–30756.

[8] J. X. Wen, E. S. Hecht, R. Mevel, Recent advances in combustion science related to hydrogen safety, Prog. Energy Combust. Sci. 107 (2025) 101202.

[9] Y. Wang, X. Guan, S. Xie, M. Zhou, Z. Zhang, Z. Chen, T. Zhang, Numerical studies on the ignition and propagation for spherically expanding premixed cool flames under gravitational conditions, Combust. Flame 259 (2024) 113194.

[10] C. K. Law, Combustion Physics, Cambridge University Press, Cambridge, 2006.

[11] M. A. Liberman, Combustion Physics: Flames, Detonations, Explosions, Astrophysical Combustion and Inertial Confinement Fusion, Springer International Publishing, Cham, 2021.

[12] P. Clavin, G. Searby, Combustion Waves and Fronts in Flows: Flames, Shocks, Detonations, Ablation Fronts and Explosion of Stars, Cambridge University Press, Cambridge, United Kingdom, 2016.

[13] M. Matalon, The Darrieus–Landau instability of premixed flames, Fluid Dyn. Res. 50 (2018) 051412.

[14] L. Yang, Y. Wang, Z. Chen, Propagation and self-acceleration of circular expanding hydrogen/air flames at cryogenic temperature, Combust. Flame 265 (2024) 113501.

[15] L. Berger, A. Attili, H. Pitsch, Intrinsic instabilities in premixed hydrogen flames: Parametric variation of pressure, equivalence ratio, and temperature. Part 1 - Dispersion relations in the linear regime, Combust. Flame 240 (2022) 111935.

[16] L. Yang, Z. Chen, Effects of cryogenic temperature on premixed hydrogen/air flame propagation in a closed channel, Proc. Combust. Inst. 39 (2023) 2991–2999.

[17] L. Yang, Y. Wang, T. Zirwes, F. Zhang, H. Bockhorn, Z. Chen, Effects of Intrinsic Instabilities on the Response of Premixed Hydrogen/Air Conical Flames to Inlet Flow Perturbations, Flow Turbulence Combust 112 (4) (2024) 1275–1297.

[18] C. Chen, C. Chi, D. Thévenin, W. Han, L. Yang, Effects of cryogenic temperature on turbulent premixed hydrogen/air flames, Proc. Combust. Inst. 40 (2024) 105749.

[19] S. Missey, O. Dounia, L. Selle, Early-stage flame acceleration in stratified hydrogen-air mixtures: Theory and simulation, Proc. Combust. Inst. 40 (2024) 105279.

[20] M. Matalon, C. Cui, J. K. Bechtold, Hydrodynamic theory of premixed flames: effects of stoichiometry, variable transport coefficients and arbitrary reaction orders, J. Fluid Mech. 487 (2003) 179–210.

[21] T. Zhang, Y. Ju, Structures and propagation speeds of autoignition-assisted premixed n-heptane/air cool and warm flames at elevated temperatures and pressures, Combust. Flame 211 (2020) 8–17.

[22] S. Mohan, M. Matalon, Numerical methodology for spontaneous wrinkling of centrally ignited premixed flames – linear theory, Combust. Theory Model. 25 (2021) 940–967.

[23] R. Addabbo, J. Bechtold, M. Matalon, Wrinkling of spherically expanding flames, Proc. Combust. Inst. 29 (2002) 1527–1535.

[24] C. E. Frouzakis, N. Fogla, A. G. Tomboulides, C. Altantzis, M. Matalon, Numerical study of unstable hydrogen/air flames: Shape and propagation speed, Proc. Combust. Inst. 35 (2015) 1087–1095.

[25] G. Sivashinsky, Nonlinear analysis of hydrodynamic instability in laminar flames—I. Derivation of basic equations, Acta Astronaut. 4 (1977) 1177–1206.

[26] D. Michelson, G. Sivashinsky, Nonlinear analysis of hydrodynamic instability in laminar flames—II. Numerical experiments, Acta Astronaut. 4 (1977) 1207–1221.

[27] Y. Rastigejev, M. Matalon, Nonlinear evolution of hydrodynamically unstable premixed flames, J. Fluid Mech. 554 (2006) 371.

[28] Y. Rastigejev, M. Matalon, Numerical simulation of flames as gasdynamic discontinuities, Proc. Combust. Inst. 10 (2006) 459–481.

[29] C. Altantzis, C. E. Frouzakis, A. G. Tomboulides, M. Matalon, K. Boulouchos, Hydrodynamic and thermodiffusive instability effects on the evolution of laminar planar lean premixed hydrogen flames, J. Fluid Mech. 700 (2012) 329–361.

[30] L. Berger, K. Kleinheinz, A. Attili, H. Pitsch, Characteristic patterns of thermodiffusively unstable premixed lean hydrogen flames, Proc. Combust. Inst. 37 (2019) 1879–1886.

[31] L. Berger, A. Attili, H. Pitsch, Intrinsic instabilities in premixed hydrogen flames: parametric variation of pressure, equivalence ratio, and temperature. Part 2 – Non-linear regime and flame speed enhancement, Combust. Flame 240 (2022) 111936.

[32] E. Hunt, A. Aspden, Thermodiffusively-unstable lean premixed hydrogen flames: Length scale effects and turbulent burning regimes, Combust. Flame 272 (2025) 113855.

[33] X. Wen, L. Berger, A. Scholtissek, A. Parente, C. Hasse, H. Pitsch, Numerical analysis and flamelet modeling of NO x formation in a thermodiffusively unstable premixed hydrogen flame at elevated-pressure conditions, Proc. Combust. Inst. 40 (2024) 105411.

[34] S. Xie, X. Chen, Y. Wang, T. Zhang, Z. Chen, Numerical study on forced ignition and flame propagation in a counterflow of nitrogen-diluted hydrogen versus air, Fuel 357 (2024) 129863.

[35] A. Attili, R. Lamioni, L. Berger, K. Kleinheinz, P. E. Lapenna, H. Pitsch, F. Creta, The effect of pressure on the hydrodynamic stability limit of premixed flames, Proc. Combust. Inst. 38 (2021) 1973–1981.

[36] L. Berger, M. Grinberg, B. Jürgens, P. E. Lapenna, F. Creta, A. Attili, H. Pitsch, Flame fingers and interactions of hydrodynamic and thermodiffusive instabilities in laminar lean hydrogen flames, Proc. Combust. Inst. 39 (2023) 1525–1534.

[37] D. G. Goodwin, R. L. Speth, H. K. Moffat, B. W. Weber, Cantera: An Object-oriented Software Toolkit for Chemical Kinetics, Thermodynamics, and Transport Processes (Aug. 2018).

[38] A. Nonaka, J. B. Bell, M. S. Day, C. Gilet, A. S. Almgren, M. L. Minion, A deferred correction coupling strategy for low Mach number flow with complex chemistry, Combust. Theory Model. 16 (2012) 1053–1088.

[39] A. A. Konnov, Yet another kinetic mechanism for hydrogen combustion, Combust. Flame 203 (2019) 14–22.

[40] A. Ghosh, N. M. Munoz-Munoz, K. P. Chatelain, D. A. Lacoste, Laminar burning velocity of hydrogen, methane, ethane, ethylene, and

propane flames at near-cryogenic temperatures, Appl. Energy Combust. Sci. 12 (2022) 100094.

[41] A. Aspden, M. Day, J. Bell, Lewis number effects in distributed flames, Proc. Combust. Inst. 33 (1) (2011) 1473–1480.

[42] J. F. Grcar, J. B. Bell, M. S. Day, The soret effect in naturally propagating, premixed, lean, hydrogen–air flames, Proc. Combust. Inst. 32 (1) (2009) 1173–1180.

[43] W. Liang, C. K. Law, Z. Chen, Ignition of hydrogen/air mixtures by a heated kernel: Role of soret diffusion, Combust. Flame 197 (2018) 416–422.

[44] S. L. Michaux, K. P. Chatelain, W. L. Roberts, D. A. Lacoste, Laminar burning velocities of hydrogen-air and methane-air flames from ambient to cryogenic temperatures at different equivalence ratios, Int. J. Hydrog. Energy 100 (2025) 608–616.

[45] D. Fernández-Galisteo, V. N. Kurdyumov, P. D. Ronney, Analysis of premixed flame propagation between two closely-spaced parallel plates, Combust. Flame 190 (2018) 133–145.

[46] J. Gaucherand, D. Laera, C. Schulze-Netzer, T. Poinsot, Intrinsic instabilities of hydrogen and hydrogen/ammonia premixed flames: Influence of equivalence ratio, fuel composition and pressure, Combust. Flame 256 (2023) 112986.

[47] J. Yuan, Y. Ju, C. K. Law, On flame-front instability at elevated pressures, Proc. Combust. Inst. 31 (2007) 1267–1274.

[48] F. Creta, P. E. Lapenna, R. Lamioni, N. Fogla, M. Matalon, Propagation of premixed flames in the presence of Darrieus–Landau and thermal diffusive instabilities, Combust. Flame 216 (2020) 256–270.

[49] T. Howarth, A. Aspden, An empirical characteristic scaling model for freely-propagating lean premixed hydrogen flames, Combust. Flame 237 (2022) 111805.

[50] L. Berger, A. Attili, H. Pitsch, Synergistic interactions of thermodiffusive instabilities and turbulence in lean hydrogen flames, Combust. Flame 244 (2022) 112254.

[51] S. Kadowaki, T. Hasegawa, Numerical simulation of dynamics of premixed flames: flame instability and vortex–flame interaction, Prog. Energy Combust. Sci. 31 (3) (2005) 193–241.

[52] M. Faghih, W. Han, Z. Chen, Effects of soret diffusion on premixed flame propagation under engine-relevant conditions, Combust. Flame 194 (2018) 175–179.